SARS-CoV-2 ORF3c suppresses immune activation by inhibiting innate sensing

Martin Müller[1], Alexandra Herrmann[2], Shigeru Fujita[3,4], Keiya Uriu[3,4], Carolin Kruth[1], Adam Strange[3], Jan Eric Kolberg[1], Markus Schneider[1], Jumpei Ito[3], Armin Ensser[2], The Genotype to Phenotype Japan (G2P-Japan) Consortium, Kei Sato[3,4,5,6,7,8], Daniel Sauter[1,3,9,*]

[1]Institute for Medical Virology and Epidemiology of Viral Diseases, University Hospital Tübingen, 72076 Tübingen, Germany

[2]Institute for Clinical and Molecular Virology, University Hospital, Friedrich-Alexander-Universität Erlangen-Nürnberg, 91054 Erlangen, Germany

[3]Division of Systems Virology, Department of Microbiology and Immunology, The Institute of Medical Science, The University of Tokyo, Minato-ku, Tokyo, Japan

[4]Graduate School of Medicine, The University of Tokyo, Minato-ku, Tokyo, Japan

[5]International Research Center for Infectious Diseases, The Institute of Medical Science, The University of Tokyo, Minato-ku, Tokyo, Japan

[6]International Vaccine Design Center, The Institute of Medical Science, The University of Tokyo, Minato-ku, Tokyo, Japan

[7]Graduate School of Frontier Sciences, The University of Tokyo, Kashiwa, Chiba, Japan

[8]CREST, Japan Science and Technology Agency, Kawaguchi, Saitama, Japan

[9]Lead contact

***Correspondence**: daniel.sauter@med.uni-tuebingen.de

ABSTRACT

SARS-CoV-2 proteins are translated from subgenomic RNAs (sgRNAs). While most of these sgRNAs are monocistronic, some viral mRNAs encode more than one protein. For example, the *ORF3a* sgRNA also encodes ORF3c, an enigmatic 41-amino acid peptide. Here, we show that ORF3c suppresses RIG-I- and MDA5-mediated immune activation and interacts with the signaling adaptor MAVS. In line with this, ORF3c inhibits IFN-β induction. This immunosuppressive activity of ORF3c is conserved among members of the subgenus sarbecovirus, including SARS-CoV and coronaviruses isolated from bats. Notably, however, the SARS-CoV-2 delta and kappa variants harbor premature stop codons in ORF3c demonstrating that this reading frame is not essential for efficient viral replication *in vivo*. In agreement with this, disruption of ORF3c did not significantly affect SARS-CoV-2 replication in CaCo-2 or CaLu-3 cells. In summary, we here identify ORF3c as an immune evasion factor that suppresses IFN-β induction, but is dispensable for efficient replication of SARS-CoV-2.

37 **INTRODUCTION**

38 Since the emergence of the COVID-19 pandemic, all canonical proteins of SARS-CoV-2 have
39 been extensively characterized for their expression, structure and function. In addition to its
40 prototypical genes, however, SARS-CoV-2 harbors several smaller open reading frames
41 (ORFs) that frequently overlap with other ORFs and may also contribute to efficient viral
42 replication. For example, the ORF3b peptide encoded by *ORF3a* subgenomic RNA (sgRNA)
43 was shown to suppress the induction of type I interferon (IFN) (Konno et al., 2020).
44 Intriguingly, naturally occurring variants of ORF3b differ in their immunosuppressive activity
45 and may be responsible for phenotypic differences between SARS-CoV and SARS-CoV-2
46 (Konno *et al.*, 2020). Moreover, several short upstream ORFs (uORFs) have been suggested to
47 regulate translation of downstream genes such as *ORF7b* (Finkel et al., 2021). Thus, non-
48 canonical ORFs of SARS-CoV-2 may also be important determinants of viral immune evasion,
49 spread and/or pathogenicity.

50 Nevertheless, most of the cryptic ORFs of SARS-Cov-2 remain poorly characterized, and
51 several open questions remain: Do they encode proteins or are they merely a result of selection
52 pressures acting on overlapping reading frames? Do these ORFs exert any regulatory activity,
53 e.g. by modulating translation of downstream ORFs via leaky scanning or ribosomal re-
54 initiation? Do they code for functional proteins that contribute to efficient immune evasion
55 and/or replication of SARS-CoV-2? Are the respective peptides or proteins immunogenic?

56 One interesting cryptic open reading frame is *ORF3c*, located at nt 25457-25579 of the Wuhan-
57 Hu-1 reference genome. This ORF was independently described by different groups and has
58 received several alternative names: ORF3c (Firth, 2020; Jungreis et al., 2021b), ORF3h (for
59 hypothetical) (Cagliani et al., 2020), 3a.iORF1 (Finkel *et al.*, 2021), and ORF3b (Pavesi, 2020).
60 Following the homology-based nomenclature proposed by Jungreis and colleagues (Jungreis et
61 al., 2021a), we will refer to this open reading frame as *ORF3c* hereafter. Like *ORF3b*, *ORF3c*
62 is one of several open reading frames overlapping with *ORF3a*. *In silico* analyses suggested

63 that the respective ORF3c protein may harbor a transmembrane domain (Firth, 2020) and act
64 as a viroporin (Cagliani *et al.*, 2020). Nevertheless, its exact function and relevance for viral
65 replication have remained unclear.
66 Here, we show that SARS-CoV-2 ORF3c encodes a stable 41-amino acid peptide that
67 suppresses the induction of IFN-β expression. Mechanistic analyses revealed that it inhibits
68 innate sensing induced by RIG-I and MDA5, and interacts with the downstream adaptor protein
69 MAVS. In line with a relevant function *in vivo*, ORF3c orthologs from different sarbecoviruses
70 share this immunosuppressive activity. However, we also identify SARS-CoV-2 lineages that
71 spread efficiently in the human population despite premature stop codons in their *ORF3c* genes.
72 Furthermore, disruption of *ORF3c* did not affect SARS-CoV-2 replication in CaCo-2 and
73 CaLu-3 cells. Thus, our findings identify ORF3c as an immune evasion factor that inhibits
74 innate sensing cascades, but is not essential for efficient viral replication.
75

76 # RESULTS

77 **SARS-CoV-2 *ORF3c* encodes a peptide suppressing IFN-β promoter activation**

78 The *ORF3a* gene of the SARS-CoV-2 reference genome Wuhan-Hu-1 overlaps with several
79 shorter open reading frames that have the potential to encode for peptides of at least 10 amino
80 acids in length (Fig. 1A). Translation initiation downstream of the start codon of *ORF3a* may
81 be enabled via non-canonical translation mechanisms, such as leaky scanning, ribosomal
82 shunting and/or re-initiation (Firth and Brierley, 2012). In line with this, the start codon of
83 ORF3c is part of a strong Kozak sequence, and *in silico* analyses predict ORF3c expression
84 from the ORF3a sgRNA via leaky scanning (Gleason et al., 2022) (Fig. 1B). Indeed, ribosome
85 profiling studies confirmed that *ORF3c* is translated in SARS-CoV-2-infected cells (Finkel *et*
86 *al.*, 2021). The same study also found evidence for translation of *ORF3d-2* (Finkel *et al.*, 2021),
87 which is in agreement with the detection of ORF3d-specific antibodies in sera from previously

88 SARS-CoV-2-infected individuals (Hachim et al., 2022). In contrast, we found no evidence for
89 antibodies against ORF3c in SARS-CoV-2 convalescent sera (Fig. S1)
90 To characterize the stability and potential activity of cryptic ORF3 peptides, we generated
91 expression vectors for the individual peptides harboring a C-terminal HA-tag (without codon-
92 optimization). Apart from the *ORF3a* construct, *ORF3c* and *ORF3d/ORF3d-2* code for stable
93 proteins that are readily detectable in transfected cells (Fig. 1C). The remaining peptides were
94 not (ORF3b-2, ORF3b-3, ORF3b-4) or only poorly (ORF3b, ORF3e) detectable. Together with
95 the ribosome profiling study and detection of antibodies in convalescent sera, this demonstrates
96 that the *ORF3a* sgRNA encodes at least three additional stable peptides, ORF3c and ORFd-2
97 in SARS-CoV-2 infected cells.
98 Since several accessory proteins of SARS-CoV-2 (e.g., ORF3b, ORF6) have been shown to
99 suppress the induction of interferons (Kimura et al., 2021; Konno *et al.*, 2020; Miorin et al.,
100 2020), we hypothesized that some of the cryptic ORF3 peptides may exert similar immune-
101 modulatory activities. Indeed, a luciferase reporter assay revealed that ORF3c significantly
102 suppresses the activation of the IFN-β promoter in response to a constitutively active mutant of
103 the pattern recognition receptor RIG-I (Fig. 1D). Notably, ORF3c was also more active than
104 the previously described IFN antagonist ORF3b, which suppressed IFN-β promoter activity
105 only at higher concentrations or upon codon-optimization (Konno *et al.*, 2020) (data not
106 shown). To test whether ORF3c is able to suppress immune activation upon viral infection, we
107 monitored endogenous *IFNB1* expression upon infection with Sendai virus (SeV), a potent
108 inducer of RIG-I-mediated type I IFN expression (Strahle et al., 2006). As expected, SeV
109 induced *IFNB1* expression in a dose-dependent manner (Fig. 1E). However, *IFNB1* mRNA
110 levels were reduced by about 70% in the presence of SARS-CoV-2 ORF3c. Together, these
111 findings demonstrate that SARS-CoV-2 *ORF3c* encodes a stable peptide that suppresses the
112 production of IFN-β upon viral sensing.
113

114 **ORF3c interacts with MAVS and suppresses both RIG-I- and MDA5-mediated immune**
115 **activation**

116 To elucidate the mechanisms underlying the inhibitory activity of ORF3, we analyzed different
117 steps of the innate RNA sensing cascade culminating in the induction of IFN-β expression (Fig.
118 2A). The *IFNB1* promoter harbors binding sites for both IRF3 and NF-κB. As expected,
119 disruption of the NF-κB binding site reduced responsiveness to RIG-I-mediated activation (Fig.
120 2B). However, ORF3c still dose-dependently reduced promoter activation (Fig. 2B),
121 demonstrating that ORF3c does not selectively target NF-κB activation. Next, we activated the
122 sensing cascade at different steps via over-expressing MDA5, MAVS or a constitutively active
123 mutant of IRF3. While ORF3c suppressed MDA5-mediated immune activation (Fig. 2C, left
124 panel), it failed to efficiently suppress *IFNB1* promoter activation in response to MAVS or IRF3
125 over-expression (Fig. 2C, middle and right panels). Together, these findings suggest that ORF3c
126 targets immune activation upstream or at the level of the signaling adaptor MAVS. In line with
127 this, SARS-CoV-2 ORF3c weakly co-immunoprecipitated with MAVS, while we found no
128 evidence for an interaction with RIG-I, MDA5 or TBK1 (Fig. 2D). The modest co-
129 immunoprecipitation of ORF3c was also observed when a MAVS mutant lacking its CARD
130 domain was used for pull-down (Fig. 2E), demonstrating that this domain is dispensable for the
131 interaction. To map residues in ORF3c involved in its immunosuppressive activity, we
132 performed an alanine scan (Fig. 2F). While all ORF3c mutants tested still reduced IFN-β
133 promoter activity, the double mutants L2A/L3A and I6A/L7A significantly reduced the
134 immunosuppressive effect of SARS-Cov-2 ORF3c. In summary, these results identify residues
135 in the N-terminus of ORF3c that contribute to its inhibitory activity and demonstrate that
136 ORF3c suppresses IFN-β expression independently of the pattern recognition receptor, i.e.
137 downstream of RIG-I and MDA5.

138

139 **The immunosuppressive activity of ORF3c is conserved among sarbecoviruses**

140 *In silico* analyses of the ORF3 locus revealed that essentially all sarbecoviruses harbor an
141 *ORF3c* gene encoding a 40- or 41-amino-acid peptide (Firth, 2020). In contrast, the remaining
142 *ORF3* genes are only poorly conserved or vary substantially in their length (Fig. 3A). The
143 absence of *ORF3c* from other subgenera of betacoronaviruses suggests that this open reading
144 frame emerged after the divergence of sarbeco- and hibecoviruses. To test whether the
145 immunosuppressive activity of ORF3c is also conserved, we characterized several orthologs
146 representing human and bat isolates of the SARS-CoV- and SARS-CoV-2-like clusters (Fig.
147 3B). Titration experiments revealed that all ORF3c peptides tested significantly suppress IFN-β
148 promoter activation (Fig. 3C). However, ORF3c of SARS-CoV-2 Wuhan Hu-1 and a closely
149 related bat coronavirus (ZXC21) suppressed IFN-β promoter activation more efficiently than
150 ORF3c of SARS-CoV Tor2 and SARS-CoV-2 BANAL-20-50. In summary, these findings
151 demonstrate that not only the *ORF3c* gene itself, but also the immunosuppressive activity of
152 the respective protein is conserved among the sarbecovirus subgenus of betacoronaviruses.
153
154 **A natural R36I polymorphism does not affect the immunosuppressive activity of ORF3c**
155 Since the emergence of SARS-CoV-2 in 2019, several mutations have occurred throughout the
156 viral genome. One notable mutation is G25563T (Fig. 4A), which is found in the beta, eta, iota
157 and mu variants and has been associated with increased transmission fitness (Oulas et al., 2021).
158 Although G25563T simultaneously introduces non-synonymous mutations in ORF3a (Q57H),
159 ORF3c (R36I) and ORF3d (E31*) (Fig. 4A), previous studies focused only on possible
160 phenotypic consequences of the Q57H change in ORF3a. Notably, however, the R36I mutation
161 in ORF3c is predicted to result in a conformational change (Fig. 4B) and a transmembrane
162 domain in the C-terminal half of ORF3c (Fig. 4C). We therefore analyzed whether the R36I
163 change may affect the subcellular localization and/or immune-suppressive activity of SARS-
164 CoV-2 ORF3c. Immunofluorescence microscopy revealed that ORF3c of the Wuhan-Hu-1
165 reference strain and a R36I mutant thereof are similarly distributed throughout the cytoplasm

166 (Fig. 4D). Moreover, both ORF3c variants dose-dependently suppressed RIG-I-mediated IFN-β
167 promoter activation to a similar extent (Fig. 4E). Thus, the G25563T polymorphism of the
168 SARS-CoV-2 beta, eta, iota and mu variants does not seem to alter the IFN-suppressive activity
169 of ORF3c.
170
171 **Some SARS-CoV-2 variants harbor premature stop codons in *ORF3c***
172 To better understand the relevance of an intact *ORF3c* gene for viral spread, we screened the
173 GISAID SARS-CoV-2 sequence repository for PANGO (sub)lineages harboring a premature
174 ORF3c stop codon in at least 20% of the isolates. We identified two mutations fulfilling these
175 criteria: the first one (C25469T) introduces a premature stop codon (Q5*) in ORF3c and an
176 S26L change in ORF3a (Fig. 4F). It is present in about 44% of B.1.617 isolates and in almost
177 all sequences of the B.1.617.1 (delta) and B.1.617.2 (kappa) sublineages (Fig. 4G). The second
178 mutation (del25498-25530) represents an in-frame deletion in ORF3a and can be found in about
179 80% of all B.1.630 isolates. This deletion results in the loss of the initiation codon of ORF3d
180 and a premature stop codon (Y14*) in ORF3c. The presence of premature ORF3c stop codons
181 in a substantial fraction of B.1.617 and B.1.630 lineages suggests that ORF3c is dispensable for
182 efficient viral replication *in vivo* and/or may be compensated by changes elsewhere in the
183 genome.
184
185 **ORF3c is dispensable for efficient SARS-CoV-2 replication**
186 To assess the importance of *ORF3c* for efficient viral replication, we generated SARS-CoV-2
187 Wuhan Hu-1 variants harboring inactivating mutations in this gene. Introducing premature stop
188 codons into *ORF3c* is not possible without simultaneously introducing non-synonymous
189 mutations in ORF3a and/or ORF3d. Using circular polymerase extension reaction (CPER)
190 (Torii et al., 2021), we therefore mutated the start codon of ORF3c to threonine (M1T), which
191 resulted in a silent mutation in the overlapping *ORF3a* gene (D22D) (Fig. 5A, left panel). After

192 rescue and validating successful introduction of the mutation, we infected CaCo-2 and CaLu-3
193 cells with an MOI of 0.1. Quantification of SARS-CoV-2 RNA copies in the culture
194 supernatants over a period of three days revealed that ORF3c M1T replicated as efficiently as
195 wild type SARS-CoV-2 (Fig. 5A, right panels). In a parallel experiment, we introduced a
196 premature stop codon (Q5*) in ORF3c, mimicking the mutation that can naturally be found in
197 the SARS-CoV-2 delta and kappa variants (Fig. 4F, 5B, left panel). Since the respective
198 nucleotide change introduces a S26L mutation in ORF3a, we simultaneously disrupted *ORF3a*
199 by introducing a premature stop codon (R6*) downstream of a methionine and potential
200 alternative start codon at position 5. While loss of ORF3a markedly reduced replicative fitness
201 in CaCo-2 cells, the virus still replicated efficiently in CaLu-3 cells (Fig. 5B, right panels). As
202 observed for the ORF3c M1T mutant, introduction of ORF3c Q5* did not significantly affect
203 the replicative fitness of the virus.
204 Since several (accessory) proteins of SARS-CoV-2 have been shown to suppress the induction
205 of IFN-β and/or IFN-β-mediated immune activation (Min et al., 2021; Xia et al., 2020), we
206 hypothesized that the immunosuppressive effect of ORF3c may be masked by other viral
207 factors. One potent suppressor of IRF3-mediated IFN-β induction is ORF6 (Kimura *et al.*, 2021;
208 Li et al., 2020). We therefore generated a BAC clone of SARS-CoV-2, in which *ORF6* was
209 replaced by a *YFP* reporter gene, and introduced the ORF3c M1T mutation described above
210 (Fig. 5C, left panel). This clone is based on the B.1 variant, and therefore additionally harbors
211 the ORF3c R36I mutation described above. Viral spread was monitored by live-cell imaging
212 and quantification of YFP-expressing (i.e. infected) cells. Again, disruption of *ORF3c* did not
213 result in impaired viral spread, and the ORF3c M1T virus replicated as efficiently as its ORF3c
214 wild type counterpart (Fig. 5C, right panels). Thus, while ORF3c and its immunosuppressive
215 activity are conserved among sarbecoviruses, the respective gene is dispensable for viral
216 replication in CaCo-2 and CaLu-3 cells.
217

218 **DISCUSSION**

219 Several lines of evidence suggested that the *ORF3c* gene of SARS-CoV-2 codes for a peptide
220 that plays a role in viral replication: (1) the respective open reading frame is conserved in
221 different sarbecoviruses and shows synonymous site conservation (Firth, 2020; Jungreis *et al.*,
222 2021b; Nelson et al., 2020) (Fig. 3), (2) upstream ATGs do not show a strong initiation context
223 and may allow ORF3c translation via leaky scanning (Firth, 2020) (Fig. 1), (3) ribosomal
224 profiling demonstrated that ORF3c is translated in SARS-CoV-2 infected cells (Finkel *et al.*,
225 2021), (4) ORF3c shows a high density of CD8+ T cell epitopes (Nelson *et al.*, 2020), (5) *in*
226 *silico* analyses predict a conserved transmembrane domain in ORF3c and a potential role as
227 viroporin (Cagliani *et al.*, 2020; Firth, 2020). Still, the exact function of ORF3c, and its
228 contribution to efficient viral replication have remained unclear.

229 Here, we identify ORF3c as an immune evasion factor of SARS-CoV-2 and other
230 sarbecoviruses that inhibits the induction of IFN-β upon activation of innate sensing cascades.
231 Using luciferase reporter assays, we demonstrate that ORF3c suppresses activation of the
232 *IFNB1* promoter by the pattern recognition receptors (PRRs) and RNA sensors RIG-I and
233 MDA5. Importantly, ORF3c also significantly reduced the expression of endogenous IFN-β in
234 response to Sendai virus infection, a known inducer of RIG-I sensing (Strahle *et al.*, 2006).
235 Since ORF3c exerts its inhibitory effect independently of the receptor, it most likely targets a
236 factor further downstream in the signaling cascade. In line with this, co-immunoprecipitation
237 experiments revealed an interaction of ORF3c with the mitochondrial signaling adaptor MAVS.
238 We found no evidence for an interaction with other components of the sensing cascade (i.e.
239 RIG-I, MDA5, or TBK1). Notably, ORF3c failed to prevent *IFNB1* promoter activation if
240 MAVS itself was used as an activator. This lack of inhibition is not merely the result of a
241 saturation effect since MAVS induced the *IFNB1* promoter less efficiently than RIG-I (Fig. 2).
242 MAVS is targeted by proteins from different viruses. For example, Influenza A Virus PB1-F2
243 inhibits innate sensing by binding to MAVS (Varga et al., 2011) and decreasing the

244 mitochondrial membrane potential (Varga et al., 2012). Another example is the NS3/4A serine
245 protease of Hepatitis C virus (HCV), which cleaves MAVS, thereby inhibiting downstream
246 immune activation (Anggakusuma et al., 2016). Similarly, SARS-CoV-2 ORF10 was recently
247 shown to induce the degradation of MAVS via mitophagy (Li et al., 2022). In contrast to HCV
248 NS3/4A and SARS-CoV-2 ORF10, however, we found no evidence for altered total protein
249 levels, proteolytic cleavage or other post-translational modifications of MAVS in the presence
250 of ORF3c. One possible mode of action may involve a competitive binding of ORF3c and RIG-
251 I/MDA5 to MAVS. In the presence of ORF3c, the CARD domain of MAVS may be blocked
252 and thus not be bound and activated by active RIG-I or MDA5. Notably, however, co-
253 immunoprecipitation experiments showed that the CARD domain of MAVS in dispensable for
254 an interaction of ORF3c with MAVS.
255 In line with a relevant role of ORF3c in viral replication, its immunosuppressive activity is
256 conserved in orthologs of other sarbecovirus species, including the SARS-CoV reference virus
257 Tor2. While all orthologs tested inhibited *IFNB1* promoter activation, those of SARS-CoV Tor2
258 and batCoV BANAL20-52 were less active than their counterparts from SARS-CoV-2 Wuhan-
259 Hu-1 and batCoV ZXC21. The reduced activity of BANAL-20-52 ORF3c can be ascribed to a
260 single amino acid change (L11P) distinguishing it from Wuhan-Hu-1 ORF3c (Fig. 3B). While
261 L11 is largely conserved in the SARS-CoV-2 cluster, most of the viruses in the SARS-CoV
262 cluster (including Tor2) harbor a glutamine at this position (Fig. 3B) (Cagliani *et al.*, 2020;
263 Firth, 2020). Thus, polymorphisms at position 11 can affect the inhibitory activity of ORF3c.
264 In addition to this, our alanine scanning approach revealed that Leu2/Leu3 and Ile6/Leu7 are
265 also contributing to the immunosuppressive effect of ORF3c. Most of these residues are
266 conserved among different sarbecoviruses. One notable exception is Ile6 (Fig. 3B). Viruses
267 from the SARS-CoV cluster harbor a Valine at this residue. These include SARS-CoV Tor2
268 ORF3c, which was less active than its SARS-CoV-2 counterpart.

269 ORF3c is not the only SARS-CoV-2 protein that interferes with RIG-I- and/or MDA-5-
270 mediated immune activation. As already mentioned above, ORF10 suppresses innate sensing
271 by targeting MAVS (Li *et al.*, 2022). Moreover, ORF3b, nucleocapsid, ORF6 and ORF8 have
272 all been shown to suppress IFN-β expression (Hayn et al., 2021; Kimura *et al.*, 2021; Konno *et*
273 *al.*, 2020; Kopecky-Bromberg et al., 2007; Li *et al.*, 2020), highlighting the selection pressure
274 exerted by this pathway. The convergent evolution of viral proteins exerting overlapping
275 immune evasion activities may represent a backup mechanism that allows viral replication even
276 if one of the IFN-β suppressing proteins is lost. In line with this, SARS-CoV-2 variants
277 expressing a C-terminally truncated, inactive ORF6 protein have emerged several times during
278 the pandemic and spread via human-to-human transmission (Kimura *et al.*, 2021). Similarly,
279 natural SARS-CoV-2 variants lacking an intact ORF3c gene still efficiently spread in the human
280 population. In fact, more than 80% of the sequenced genomes of B.1.617.1, B.1.617.2 and
281 B.1.630 harbor premature stop codons at positions 5 and 15, respectively (Fig. 4). We
282 hypothesized that the loss of ORF3c in these viruses may be compensated by the activity of
283 ORF6. However, replication kinetics in CaCo-2 and CaLu-3 cells revealed that loss of ORF3c
284 does not affect viral replication in the absence of ORF6 either (Fig. 5). Intriguingly, IFN-β
285 mRNA was not detectable in cells infected with the SARS-CoV-2 double mutant lacking
286 ORF3c and ORF6 (data not shown). Thus, yet another viral inhibitor of IFN-β expression (e.g.
287 ORF8 or N) may be able to rescue efficient viral replication in this case.
288 Notably, the emergence of premature stop codons in small reading frames such as *ORF3c* may
289 also be tolerated or even be beneficial if they provide a fitness advantage by optimizing
290 overlapping reading frames. For example, the ORF3c Q5* mutation is accompanied by an S26L
291 change in ORF3a. However, experimental disruption of ORF3c without changing the amino
292 acid sequence of ORF3a (Fig. 5A) or upon deletion of ORF3a (Fig. 5B) did not affect viral
293 replication *in vitro* either.

294 One intriguing observation is the emergence of a nucleotide change in a subfraction (~3%) of
295 B.1.617.2 viruses that reverts the stop codon at position 5 to a tyrosine (*5Y). Thus, it is
296 tempting to speculate that the loss of ORF3c was initially just carried along with mutations
297 elsewhere in the genome (e.g. in Spike) that conferred a major fitness advantage to the virus,
298 before ORF3c expression was reverted by another point mutation.
299 In summary, our study identifies ORF3c as an immune evasion factor of SARS-CoV-2 and
300 other sarbecoviruses. While an intact ORF3c gene is clearly dispensable for viral replication *in*
301 *vitro* and *in vivo*, the conservation of this short open reading frame and the pseudo-reversion of
302 premature stop codons suggests that it may still contribute to efficient viral replication *in vivo*.
303 The emergence of future SARS-CoV-2 variants may help to fully decipher the role of this
304 enigmatic ORF and its co-evolution with other viral genes.
305

306 **ACKNOWLEDGMENTS**

307 We thank Isabell Haußmann for excellent technical assistance and would like to thank the
308 following persons for providing helpful reagents: Peter D Burbelo (LIPS assay plasmids),
309 Konstantin MJ Sparrer (RIG-I, MDA5 and TBK1 expression plasmids, IRF luciferase reporter
310 plasmid), Harmit Malik (MAVS expression plasmid), Rongtuan Lin (IRF3 expression plasmid),
311 Bernd Baumann (NF-κB luciferase reporter plasmid, *Gaussia* luciferase control vector, IKKβ
312 expression plasmid), Michael Gale Jr (IFN-β promoter reporter plasmid), Prof. Takasuke
313 Fukuhara (CPER plasmids and cell lines) and Prof. Takashi Irie (pCAGGS Flag-IRF3 5d).
314 SARS-CoV-2 mNeon Green was kindly provided by Prof. Michael Schindler. This work was
315 funded by the Federal Ministry of Education and Research Germany (BMBF; grant ID: FKZ
316 01KI20135), the Canon Foundation Europe, the Heisenberg Program of the German Research
317 Foundation (DFG; grant ID: SA 2676/3-1) and grants of the COVID-19 program of the Ministry
318 of Science, Research and the Arts Baden-Württemberg (MWK; grants IDs: MWK K.N.K.C.014
319 (U21) and MWK K.N.K.C.015 (U22)) to D.S. AE and AH were supported by BMBF

320 SenseCoV2 01KI20172A; DFG Fokus COVID-19, EN 423/7-1; and Coronavirus research
321 grants by the Bavarian State Ministry of Science and the Arts and Bavarian State Ministry of
322 Health, Bay-VOC.
323

324 AUTHOR CONTRIBUTIONS

325 M.M. and D.S. conceptualized the study and designed the experiments. M.M. performed most
326 of the experiments. A.H. and A.E. generated and provided BAC clones for SARS-CoV-2
327 ΔORF6 YFP (ORF3c wild type and ΔORF3). S.F. and D.S. generated SARS-CoV-2 mutants
328 via CPER that were characterized by D.S., S.F. and K.U., C.K. and J.E.K. performed some of
329 the luciferase reporter assays. M.S. sequenced the YFP reporter viruses. A.S. and J.I. performed
330 *in silico* analyses to identify premature stop codons in ORF3c. M.M. and D.S. prepared the
331 figures, and D.S. wrote the initial draft of the manuscript. All authors reviewed and edited the
332 manuscript. A.E., K.S. and D.S. supervised the experiments, provided resources and acquired
333 funding.
334

335 DECLARATION OF INTERESTS

336 The authors declare no competing interests.
337

338 MATERIAL AND METHODS

339 Cell lines

340 HEK293T were maintained in Dulbecco's modified Eagle medium (DMEM) supplemented
341 with 10% heat-inactivated fetal calf serum (FCS), L-glutamine (2 mM), streptomycin (100
342 mg/ml) and penicillin (100 U/ml) and were cultured at 37°C, 90% humidity and 5% CO_2. They
343 were isolated from a female fetus. HEK293T cells were transfected using a standard calcium
344 phosphate method. HEK293-C34 cells, IFNAR1 KO HEK293 cells expressing human ACE2

345 and TMPRSS2 by doxycycline treatment (Torii *et al.*, 2021), were maintained in DMEM (high
346 glucose) containing 10% FBS, 10 mg/ml blasticidin (InvivoGen) and 1% PS. Caco-2 (human
347 colorectal adenocarcinoma, male) cells were grown in Dulbecco's modified Eagle's medium
348 (DMEM) supplemented with 10% heat-inactivated FCS, 100 units/ml penicillin, 100 µg/ml
349 streptomycin, 2 mM L-glutamine, and 1x non-essential amino acids (NEAA). Calu-3 cells (lung
350 adenocarcinoma, male) were cultured in Eagle's minimum essential medium (EMEM)
351 supplemented with 20% heat-inactivated FCS, 100 units/ml penicillin, and 100 µg/ml
352 streptomycin. Medium was changed every day. Vero E6 (*Cercopithecus aethiops* derived
353 epithelial kidney, female) cells were grown in Dulbecco's modified Eagle's medium (DMEM)
354 supplemented with 2.5% heat-inactivated FCS, 100 units/ml penicillin, 100 µg/ml
355 streptomycin, 2 mM L-glutamine, 1 mM sodium pyruvate, and 1x non-essential amino acids.
356 Derivatives thereof stably expressing TMPRSS2 were cultured in (DMEM) supplemented with
357 5% heat-inactivated FCS, 100 units/ml penicillin, 100 µg/ml streptomycin, and 100 µg/ml
358 G418.
359
360 Virus strains and virus propagation
361 SARS-CoV-2 ΔORF6-YFP and SARS-CoV-2 ΔORF6-YFP ΔORF3c were propagated by
362 inoculation of Vero E6/TMPRSS2 cells in 75 cm² cell culture flasks in medium containing 2%
363 FCS. Cells were incubated at 37°C and supernatants were harvested 2 to 4 days post inoculation.
364 Supernatants were centrifuged for 5 min at 1,000 × g to remove cellular debris, and then
365 aliquoted and stored at -80°C as virus stocks. Infectious titer was determined in Vero
366 E6/TMPRSS2 cells as Tissue Culture Infection Dose 50 ($TCID_{50}$)/ml (see Method Details).
367
368 *In silico* prediction of translation initiation sites
369 Translation initiation sites (TIS) and Kozak context were determined using TIS predictor
370 (https://www.tispredictor.com/) (Gleason *et al.*, 2022).

371

372 *In silico* prediction of ORF3c secondary structure and transmembrane domains

373 To predict the secondary structure of ORF3c and its R36I variant PEP-FOLD 3 (Camproux et
374 al., 2004) was used.

375 The effect of point mutations on a transmembrane domain in ORF3c was predicted using the
376 'Prediction of transmembrane helices in proteins' tool TMHMM2.0 (Sonnhammer *et al.*, 1998).

377

378 Generation of expression plasmids

379 ORF3c genes were PCR-amplified using viral cDNA as a template and subsequently inserted
380 into a pCG expression vector co-expressing GFP via an IRES using unique XbaI and MluI
381 restriction sites. To facilitate protein detection, a C-terminal HA-tag
382 (TACCCATACGATGTTCCAGATTACGCT) was added by extension PCR. To generate
383 ORF3c-HA alanine mutants as well as ORF3c-R36I, -BANAL-20-52, -Tor2 and SL-
384 CoVZXC21, point mutations were introduced by site-directed mutagenesis using the wild type
385 Wuhan-Hu-1 ORF3c-HA expression plasmid as template. pRen2-ORF3c was generated by
386 conventional cloning, using the unique EcoRI and XhoI restriction sites in pRen2. IRF3 5D was
387 PCR-amplified using pCAGGS Flag-IRF3 5D as a template and subsequently inserted into
388 pEGFP-C1 via XhoI and EcoRI. All constructs were sequenced to verify their integrity. PCR
389 primers are listed in the Key Resources Table.

390

391 Generation and recovery of a recombinant SARS-CoV-2 ORF3 mutant

392 Stop mutations within ORF3c were introduced into the bacmid pBSCoV2_d6-YFP harboring
393 the SARS-CoV-2 backbone (Herrmann et al., 2021) using 2-step Red Recombination (Tischer
394 et al., 2006). For this purpose, the KanS cassette was amplified from pEP-KanS with the
395 following oligonucleotides:

396 (1) mut3c-fwd: caattggaactgtaactttgaagcaaggtgaaatcaaggaCgctactccttcagattttgAGGATGACG
397 ACGATAAGTAGGG
398 (2) mut3c-rev: gtatcgttgcagtagcgcgaacaaaatctgaaggagtagcGtccttgatttcaccttgctCAACCAATT
399 AACCAATTCT GATTAG
400 Integrity of the obtained bacterial artificial chromosomes (BAC) and presence of desired stop
401 mutations were confirmed by restriction digestion and next generation sequencing.
402 Recombinant SARS-CoV-2 viruses expressing EYFP instead of the viral ORF6 protein and
403 containing mutations within ORF3c were recovered by transfection of the BACs into HEK293T
404 cells overexpressing viral N protein, ACE2 receptor, and T7 RNA polymerase as described
405 previously (Herrmann *et al.*, 2021). The obtained reporter viruses were further passaged on
406 CaCo-2 cells and viral titers were determined by endpoint titration (see $TCID_{50}$).
407
408 <u>Generation of recombinant SARS-CoV-2 mutants by circular polymerase extension reaction</u>
409 To generate recombinant SARS-CoV-2 by circular polymerase extension reaction (CPER)
410 (Torii *et al.*, 2021) nine DNA fragments comprising parts of SARS-CoV-2 (WK-521, PANGO
411 lineage A; GISAID ID: EPI ISL 408667) (Matsuyama et al., 2020) were generated by PCR
412 using PrimeSTAR GXL DNA polymerase. A linker fragment comprising hepatitis delta virus
413 ribozyme, the bovine growth hormone poly A signal and the cytomegalovirus promoter was
414 also prepared by PCR. The ten obtained DNA fragments were mixed and used for
415 CPER. ORF3c mutations were inserted in fragment 9/10 by site-directed overlap extension
416 PCR with the primers listed in the key resources table.
417 To produce chimeric recombinant SARS-CoV-2, Tetracycline-inducible ACE2 and TMPRSS-
418 expressing IFNAR1-deficient HEK293 (HEK293-C34) cells were transfected with the CPER
419 products using TransIT-LT1 according to the manufacturer's protocol. One day post
420 transfection, the culture medium was replaced with Dulbecco's modified Eagle's medium (high
421 glucose) containing 2% FCS, 1% PS and doxycycline. At 7 d post transfection, the culture

422 medium was harvested and centrifuged, and the supernatants were collected as the seed virus.
423 To remove the CPER products (i.e., any SARS-CoV-2 DNA), 1 ml of the seed virus was treated
424 with 2 µl TURBO DNase (Thermo Fisher Scientific, Cat# AM2238) and incubated at 37°C for
425 1 h. Complete removal of the CPER products (i.e., SARS-CoV-2-related DNA) from the seed
426 virus was verified by PCR.
427 To prepare virus stocks for infection, VeroE6/TMPRSS2 cells (5,000,000 cells in a T-75 flask)
428 were infected with 20-50 µl of the seed virus. One-hour post infection, the culture medium was
429 replaced with DMEM (low glucose) containing 2% FBS and 1% PS. Two to four days post
430 infection, the culture medium was harvested and centrifuged, and the supernatants were
431 collected. Viral titers were determined by $TCID_{50}$. To verify the sequence of chimeric
432 recombinant SARS-CoV-2, viral RNA was extracted from the virus stocks using the QIAamp
433 viral RNA mini kit and viral genomes were sequenced as described before (Kimura et al., 2022).
434
435 Tissue culture infectious dose ($TCID_{50}$)
436 Viral titers were determined as the 50% tissue culture infectious dose. Briefly, one day before
437 infection, VeroE6/TMPRSS2 cells (10,000 cells) were seeded into 96-well plates. Cells were
438 inoculated with serially diluted virus stocks and incubated at 37°C. Four days later, cells were
439 checked microscopically for cytopathic effects (CPE), and $TCID_{50}$/ml was calculated using the
440 Reed–Muench method.
441
442 SARS-CoV-2 replication kinetics in Vero E6, Caco-2 and Calu-3 cells
443 One day before infection with CPER-derived SARS-CoV-2 clones, Caco-2 cells (10,000
444 cells/well) or CaLu-3 cells (20,000 cells/well) were seeded into a 96-well plate. Cells were
445 infected with SARS-CoV-2 at an MOI of 0.1 and incubated at 37°C. One hour later, the infected
446 cells were washed and 180 µl of culture medium was added. The culture supernatants and cells
447 were harvested at the indicated timepoints and used for RT–qPCR to quantify the viral RNA

448 copy number. For replication kinetics of BAC-derived SARS-CoV-2 ΔORF6-YFP and SARS-
449 CoV-2 ΔORF6-YFP ΔORF3c, Caco-2 cells (10,000/well) were seeded into a 96-well plate one
450 day prior to infection. Cells were infected in triplicates at an MOI of 0.1 & 0.01 for 1 hour at
451 37°C. After washing and addition of 100 µl fresh culture medium the plates were placed in an
452 Incucyte plate reader and images were taken at the indicated time points for up to 96 hours.
453 The 'Basic Analysis Mode' was applied to quantify virus growth as green area normalized to
454 phase area. Supernatants and cells were harvested at the indicated time points to determine
455 cytokine levels by Cytokine Array and RT-qPCR respectively.
456
457 RT–qPCR
458 5 µl culture supernatant was mixed with 5 µL of 2 x RNA lysis buffer [2% Triton X-100,
459 50 mM KCl, 100 mM Tris-HCl (pH 7.4), 40% glycerol, 0.8 U/µL recombinant RNase inhibitor
460 and incubated at room temperature for 10 minutes. RNase-free water (90 µL) was added, and
461 the diluted sample (2.5 µl) was used as the template for real-time RT-PCR performed according
462 to the manufacturer's protocol using the OneStep TB Green PrimeScript PLUS RT-PCR kit
463 and the following primers: Forward *N*, 5′-AGC CTC TTC TCG TTC CTC ATC AC-3′; and
464 Reverse *N*, 5′-CCG CCA TTG CCA GCC ATT C-3′. The viral RNA copy number was
465 standardized using a home-made standard.
466 *IFNB1* and *IL6* RNA levels were determined in cell lysates collected from (1) SARS-CoV-2
467 ΔORF6-YFP and SARS-CoV-2 ΔORF6-YFP ΔORF3c infected CaCo-2 wild-type cells and (2)
468 transfected HEK293T cells infected with Sendai virus for 8 hours. Total RNA was isolated
469 using the Viral RNA Mini Kit (Qiagen) according to the manufacturer's instructions. Genomic
470 DNA was removed using the DNA-free kit (Thermo Fischer Scientific) and subsequent cDNA
471 synthesis was performed using the PrimeScript RT reagent Kit (TAKARA), both according to
472 the manufacturer's instructions. qPCR was performed using the Luna Universal Probe qPCR
473 Master Mix (NEB) together with primer probes for IFN-β, IL-6 and GAPDH (Thermo Fischer

474 Scentific). All reactions were run in duplicates and RNA levels were internally normalized to
475 GAPDH.
476
477 Transfection of HEK293T cells
478 For overexpression experiments, HEK293T cells were transfected using standard calcium
479 phosphate transfection protocols. 6x 10^5 cells were seeded in 6-well plates on the day before
480 and medium was changed 6 hours after transfection.
481
482 Co-immunoprecipitation
483 To investigate possible interactions between ORF3c and proteins of the Interferon signaling
484 pathway, co-immunoprecipitation with subsequent analysis by western blotting was performed.
485 Briefly, HEK293T cells were seeded in 6-well plates and co-transfected with expression
486 plasmids for HA-tagged ORF3c and Flag-tagged RIG-I, MDA5, MAVS or TBK1 (ratio 4:1;
487 5µg/well). One day post transfection, cells were lysed in 300 µl western blot lysis buffer and
488 cleared by centrifugation (see "Western blotting"). 45 µl of the lysate was used for whole-cell
489 lysate analysis and further prepared as described in "Western blotting", while 255 µl of the
490 lysate was used for co-immunoprecipitation. A pre-clearing step was performed to remove
491 unspecifically binding compounds from the lysate. Pierce Protein A/G Magnetic beads (Thermo
492 Fisher) were washed three times with 1 ml NP40 wash buffer (50 mM HEPES, 300 mM NaCl,
493 0.5% NP40, pH 7.4) and added to the lysate. After incubation for 1 h at 4°C, beads were
494 removed from the lysate using a magnetic rack. To precipitate protein complexes, the lysate
495 was incubated first with an anti-Flag antibody (Sigma, 1.5 µg/sample) for 1 hour followed by
496 addition of 15 µl washed Protein A/G Magnetic Beads for one additional hour at 4°C. After
497 incubation, the beads were washed three times in NP40 wash buffer before incubation with
498 80 µl 1 x Protein Sample Loading Buffer at 95°C for 10 minutes to recover bound proteins.

499 After addition of 1.75 ml β-mercaptoethanol, whole-cell lysates and precipitates were analyzed
500 by western blotting.
501
502 Western blotting
503 To determine expression of cellular and viral proteins, cells were washed in PBS, lysed in
504 western blot lysis buffer (150 mM NaCl, 50 mM HEPES, 5 mM EDTA, 0.1% NP40, 500 mM
505 Na3VO4, 500 mM NaF, pH 7.5) and cleared by centrifugation at 20,800 x g for 20 min at 4°C.
506 Lysates were mixed with Protein Sample Loading Buffer (LI-COR) supplemented with 10% β-
507 mercaptoethanol and heated at 95°C for 5 min. Proteins were separated on NuPAGE 4%–12%
508 Bis-Tris Gels (Thermo Fischer Scientific), blotted onto Immobilon-FL PVDF membranes and
509 stained using primary antibodies directed against HA-tag, Flag-tag, GAPDH, RIG-I, MDA5,
510 MAVS, TBK1, IRF3 and Infrared Dye labeled secondary antibodies (LI-COR IRDye). Proteins
511 were detected using a LI-COR Odyssey scanner and band intensities were quantified using LI-
512 COR Image Studio Lite Version 5.2.
513
514 Immunofluorescence microscopy
515 Confocal immunofluorescence microscopy was used to determine the subcellular localization
516 of ORF3c and ORF3c R36I. Briefly, 150,000 HEK293T cells were seeded on 13 mm diameter
517 glass coverslips coated with poly-L-lysine (Sigma-Aldrich) in 24-well plates. On the following
518 day, cells were transfected with an expression plasmid for ORF3c, ORF3c R36I or an empty
519 vector control (500 ng) using Lipofectamin2000 (Invitrogen). One day post transfection, cells
520 were fixed in 4% PFA for 20 min at RT, permeabilized in PBS 0.5% Triton X-100 for 15 min
521 at RT and blocked in 5% BSA/PBS supplemented with 0,1% Triton X-100 for 15 min at RT.
522 ORF3c was stained using a primary antibody against the HA-tag and secondary goat anti-mouse
523 AF555. Nuclei were stained in parallel using 4′,6-Diamidine-2′-phenylindole (DAPI; Thermo

524 Fischer Scientific). Coverslips were mounted on glass slides using Mowiol (CarlRoth)
525 mounting medium and confocal microscopy was performed using an LSM710 (Carl Zeiss).
526
527 Firefly luciferase assay
528 HEK293T cells were seeded in 96 well plates at $3x10^4$ cells /well. After 24 h, cells were
529 transfected with a mix of expression vectors containing firefly luciferase reporter constructs for
530 the IFN-β promoter or a mutant thereof lacking NF-κB biding sites (IFN-β ΔNF-κB) (reporter,
531 10 ng), a *Gaussia* luciferase expression plasmid (normalization control, 5 ng), expression
532 plasmids for RIG-I-CARD, MDA5, MAVS or IRF3 5D (stimulus, 5 ng), different amounts of
533 ORF3 expression constructs (12.5 - 100 ng) and empty vector (pCG_HIV-1 M NL4-3 *nef* stop
534 ΔIRES-eGFP) to adjust total DNA amounts across all conditions to 200 ng/well. After 24 h,
535 supernatants were harvested, and cells were lysed in 100µl 1x Passive Lysis Buffer (Promega).
536 *Gaussia* luciferase activity in the supernatants was measured by addition of Coelenterazine
537 (PJK Biotech). Firefly luciferase activity was measured in the cells using the Luciferase Assay
538 System (Promega) according to the manufacturers instruction.
539
540 LIPS assay
541 Luciferase fusion protein (10^6 RLU) in 50 µl Buffer A (50 mM Tris, 150 mM NaCl, 0.1% Triton
542 X-100, pH 7.5) and 1 µl sample serum in 49 µl Buffer A was added to 1.5 ml tubes and
543 incubated with shaking at 300 rpm for 1 h at room temperature. Pierce Protein A/G Magnetic
544 beads were added to each condition as a 30% suspension in PBS for an additional hour and
545 shaking at room temperature. Samples were placed on a magnetic rack, and supernatant was
546 removed after 1-minute incubation. Magnetic beads were washed twice with 150 µl Buffer A
547 followed by 2 washes with 150 µl PBS. Samples were transferred into a 96-well opaque nunc-
548 plate (VWR), and 50 µl Coelenterazine (PJK Biotech) was added to each condition. Samples

549 were measured immediately on a TriStar² S LB 942 Multimode Reader (Berthold Technologies)
550 with an integration time of 0.1 seconds and a read height of 1 mm.
551
552 **QUANTIFICATION AND STATISTICAL ANALYSIS**
553 Statistical analyses were performed using GraphPad PRISM 9.4.1. For statistical testing
554 between two means P values were calculated using paired or unpaired Student's t test. For
555 comparison within one group, we used one-way analysis of variation (ANOVA) with Dunnett's
556 multiple comparison test and for comparison between two or more groups we used two-way
557 ANOVA with Sidak's multiple comparison test. Unless otherwise stated, data are shown as the
558 mean of at least three independent experiments ± SD. Significant differences are indicated as:
559 * $p \leq 0.05$; ** $p \leq 0.01$; *** $p \leq$ % 0.001 and **** $p \leq 0.0001$. Statistical parameters are
560 specified in the figure legends.
561
562 **FIGURE LEGENDS**
563 **Figure 1: Open reading frames in the *ORF3* gene locus and inhibition of IFN-β induction**
564 **by SARS-CoV-2 ORF3c. (A)** Genome organization of SARS-CoV-2 is illustrated on top;
565 overlapping ORFs in the ORF3 locus are shown at the bottom. Vertical grey lines indicate
566 internal ATG codons. Experimentally confirmed translation initiation sites (Finkel *et al.*, 2021)
567 are highlighted by grey triangles. **(B)** Kozak sequences of the *ORF3c* initiation codon and
568 upstream ATG codons in *ORF3a* are shown. ATG context was determined using TIS predictor
569 (https://www.tispredictor.com/) (Gleason *et al.*, 2022). **(C)** Western blot analysis of HEK293T
570 cells transfected with two different concentrations of expression plasmids for the indicated
571 ORF3 proteins and peptides. ORF3a to ORF3e were detected via a C-terminal HA tag. GAPDH
572 served as loading control. **(D)** HEK293T cells were co-transfected with the indicated ORF3
573 expression plasmids, a reporter plasmid expressing firefly luciferase under the control of the
574 *IFNB1* promoter and a construct expressing *Gaussia* luciferase under the control of a minimal

575 promoter. To induce immune signaling, half of the samples were additionally co-transfected
576 with an expression plasmid for the CARD domain of RIG-I. One day post transfection, firefly
577 luciferase activity was determined and normalized to *Gaussia* luciferase activity. Mean values
578 of three independent experiments measured in triplicates (±SD) are shown. **(E)** HEK293T cells
579 were transfected with an expression plasmid for SARS-CoV-2 ORF3c or an empty vector
580 control. 24 hours post transfection, cells were infected with increasing amounts of Sendai virus
581 (SeV) for an additional 8 hours. Cells were lysed to perform either RNA extraction and
582 subsequent qPCR for IFN-β (left panel) or western blot analysis (right panel). Mean values of
583 three independent experiments measured in duplicates (±SD) are shown. Multiple comparison
584 within individual reporter assays (D) were determined by one-way ANOVA with Dunnett's
585 test; * $p \leq 0.05$; ** $p \leq 0.01$; *** $p \leq$ % 0.001 and **** $p \leq 0.0001$. Multiple comparison
586 between groups (E) were determined by two-way ANOVA with Sidak's multiple comparison
587 test; * $p \leq 0.05$; ** $p \leq 0.01$; *** $p \leq$ % 0.001 and **** $p \leq 0.0001$.
588
589 **Figure 2. ORF3c interacts with MAVS and inhibits IFN-β induction independently of the**
590 **pattern recognition receptor. (A)** Cartoon illustrating IRF3- and NF-κB-mediated activation
591 of the *IFNB1* promoter upon RIG-I- or MDA5-mediated sensing. **(B)** HEK293T cells were co-
592 transfected with increasing amounts of an expression plasmid for SARS-CoV-2 ORF3c, a
593 construct expressing *Gaussia* luciferase under the control of a minimal promoter and a reporter
594 plasmid expressing firefly luciferase under the control of the *IFNB1* promoter (left panel) or a
595 mutant thereof lacking the NF-κB binding site (right panel). Immune signaling was induced by
596 co-transfecting an expression plasmid for the CARD domain of RIG-I. One day post
597 transfection, firefly luciferase activity was determined and normalized to *Gaussia* luciferase
598 activity. Mean values of three independent experiments measured in triplicates (±SD) are
599 shown. **(C)** HEK293T cells were transfected and analyzed essentially as described in (B).
600 Instead of RIG-I CARD, however, immune signaling was introduced by co-transfecting

601 expression plasmids for MDA5 (left panel), MAVS (central panel) or a constitutively active
602 mutant of IRF3 (right panel). Mean values of three independent experiments measured in
603 triplicates (±SD) are shown. **(D, E)** HEK293T cells were co-transfected with expression
604 plasmids for (D) Flag-tagged RIG-I, MDA5, MAVS, TBK1, (E) MAVS or a mutant thereof
605 lacking its CARD domain (MAVSΔCARD) and an expression plasmid for HA-tagged SARS-
606 CoV-2 ORF3c. One day post transfection, cells were lysed. Cell lysates were analyzed by
607 Western blotting, either directly ("input") or upon pull-down using a Flag-specific antibody
608 ("IP"). **(F)** HEK293T cells were co-transfected with expression plasmids as described in (B,
609 left panel). Immune signaling was induced by co-transfecting an expression plasmid for the
610 CARD domain of RIG-I as well as the indicated ORF3c alanine mutants. Multiple comparison
611 within individual reporter assays (B, C, F) were determined by one-way ANOVA with
612 Dunnett's test; * $p \leq 0.05$; ** $p \leq 0.01$; *** $p \leq$ % 0.001 and **** $p \leq 0.0001$.
613
614 **Figure 3. Conservation of ORF3c and its immunosuppressive activity in sarbecoviruses.**
615 **(A)** Simplified cartoon illustrating the *ORF3* locus of randomly selected members of the
616 *Sarbeco*-, *Hibeco*- and *Nobecovirus* genera. Open reading frames with a length of at least 30
617 nucleotides are indicated as rectangles. ORF3c is highlighted in dark red. **(B)** Alignment of
618 ORF3c amino acid sequences of the indicated viral isolates. Members of the SARS-CoV-2
619 cluster are shown on top, members of the SARS-CoV cluster at the bottom. For the underlined
620 ORF3c sequences, expression plasmids were generated and analyzed for their ability to inhibit
621 *IFNB1* promoter activation in **(C)**. Briefly, HEK293T cells were co-transfected with increasing
622 amounts of the indicated ORF3c expression plasmids, a reporter plasmid expressing firefly
623 luciferase under the control of the *IFNB1* promoter and a construct expressing *Gaussia*
624 luciferase under the control of a minimal promoter. An expression plasmid for Influenza A virus
625 non-structural protein 1 (NS1) served as positive control. Immune signaling was induced by co-
626 transfecting an expression plasmid for the CARD domain of RIG-I. One day post transfection,

627 firefly luciferase activity was determined and normalized to *Gaussia* luciferase activity. Mean
628 values of three independent experiments measured in triplicates (±SD) are shown. Multiple
629 comparison between groups (C) were determined by two-way ANOVA with Sidak's multiple
630 comparison test; ns not significant, * $p \leq 0.05$; ** $p \leq 0.01$; *** $p \leq$ % 0.001 and **** $p \leq$
631 0.0001.
632
633 **Figure 4. Characterization of naturally occurring variants of SARS-CoV-2 ORF3c. (A)**
634 Cartoon illustrating non-synonymous changes in ORF3a, c and d as a result of the naturally
635 occurring polymorphisms G25563T. **(B)** Secondary structure of Wuhan Hu-1 ORF3c (red) and
636 the respective R36I variant thereof (blue) as predicted using PEP-FOLD 3 (Camproux et al.,
637 2004). **(C)** The presence of transmembrane domains in Wuhan Hu-1 ORF3c (left panel) and
638 the respective R36I variant thereof (right panel) was predicted using TMHMM - 2.0 (Krogh et
639 al., 2001). **(D)** HEK293T cells were transfected with expression plasmids for Wuhan Hu-1
640 ORF3c or ORF3c R36I. One day post transfection, cells were stained for ORF3c (anti-HA,
641 green) and nuclei (DAPI, blue) (scale bar = 20 µm). **(E)** HEK293T cells were co-transfected
642 with increasing amounts of the indicated ORF3c expression plasmids, a reporter plasmid
643 expressing firefly luciferase under the control of the *IFNB1* promoter and a construct expressing
644 *Gaussia* luciferase under the control of a minimal promoter. Immune signaling was induced by
645 co-transfecting an expression plasmid for the CARD domain of RIG-I. One day post
646 transfection, firefly luciferase activity was determined and normalized to *Gaussia* luciferase
647 activity. Mean values of three independent experiments measured in triplicates (±SD) are
648 shown. **(F)** Mutations introducing premature stop codons in ORF3c that can be found in at least
649 20% of the samples of at least one PANGO (sub)lineage. **(G)** Frequency of the mutations shown
650 in (F) in the PANGO (sub)lineages B.1.617.1 (delta), B.1.617.2 (kappa), B.1.617 and B.1.630.
651 Multiple comparison between groups (E) were determined by two-way ANOVA with Sidak's
652 multiple comparison test; ns, not significant.

653

654 **Figure 5. Disruption of ORF3c does not affect SARS-CoV-2 replication in CaCo-2 or**
655 **CaLu-3 cells. (A)** Circular polymerase extension reaction (CPER) was used to disrupt the start
656 codon of ORF3c (M1T) in SARS-CoV-2 without affecting the amino acid sequence of ORF3a
657 (left panel). CaCo-2 and CaLu-3 cells were infected with ORF3c wild type (red) or ORF3c-
658 mutated (blue) SARS-CoV-2 at an MOI of 0.1. Viral replication was monitored over 72 hours
659 by determining viral RNA copies in the culture supernatants (right panels). Mean values of four
660 independent experiments (±SD) are shown. **(B)** CPER was used to introduce a premature stop
661 codon in ORF3c (Q5stop). To avoid any bias by simultaneously changing the protein sequence
662 of ORF3a (S26L), a premature stop codon was also inserted in ORF3a (R6*) (left panel). Viral
663 replication (right panels) was monitored in CaCo-2 and CaLu-3 cells as described in (A). Mean
664 values of four independent experiments (±SD) are shown. **(C)** A SARS-CoV-2 BAC clone
665 harboring a disrupted ORF3c (M1T) and expressing YFP instead of ORF6 was generated (left
666 panel). CaCo-2 cells were infected with SARS-CoV-2 ΔORF6-YFP (red) or SARS-CoV-2
667 ΔORF6-YFP ΔORF3c (blue) at an MOI of 0.1 (middle panel) or 0.01 (right panel). Cells were
668 placed in a live cell imaging device, and the area of YFP positive cells over the total area of
669 cells was quantified every 4 hours for 96 hours. Images below graphs show continuous virus
670 spread (green) over the indicated time points from one randomly chosen well. Graphs show
671 mean values of 3 independent experiments performed in triplicates (±SD). Multiple comparison
672 between groups (A-C, right panel) were determined by two-way ANOVA with Sidak's multiple
673 comparison test; * $p \leq 0.05$; ** $p \leq 0.01$; *** $p \leq$ % 0.001 and **** $p \leq 0.0001$.

674

675 ## SUPPLEMENTAL INFORMATION

676 **Figure S1: Detection of SARS-CoV-2-specific antibodies via Luciferase**
677 **Immunoprecipitation System (LIPS). (A)** Principle of the LIPS assay: HEK293T cells are
678 transfected with expression plasmids for a viral protein of interest fused to *Renilla* luciferase.

679 Subsequently, transfected cells are lysed and incubated with serum samples and magnetic
680 beads. Antibodies against viral proteins of interest will cross-link the luciferase-containing
681 proteins with beads and allow magnet-assisted pull-down of both beads and luciferase activity.
682 **(B)** LIPS-mediated quantification of antibodies against SARS-CoV-2 N (left panel) and ORF3c
683 (right panel) in sera from SARS-CoV-2 naïve and convalescent sera (RLU, relative light units).
684 Each dot represents one independent serum sample. Differences in antibody levels between
685 SARS-CoV-2 naïve and convalescent sera was determined by unpaired student's t-test with
686 Welch's correction; * $p \leq 0.05$, ** $p \leq 0.01$, *** $p \leq 0.001$.
687

688 **REFERENCES**
689

690 Anggakusuma, Brown, R.J.P., Banda, D.H., Todt, D., Vieyres, G., Steinmann, E., and
691 Pietschmann, T. (2016). Hepacivirus NS3/4A Proteases Interfere with MAVS Signaling in both
692 Their Cognate Animal Hosts and Humans: Implications for Zoonotic Transmission. J Virol *90*,
693 10670-10681. 10.1128/JVI.01634-16.
694 Cagliani, R., Forni, D., Clerici, M., and Sironi, M. (2020). Coding potential and sequence
695 conservation of SARS-CoV-2 and related animal viruses. Infect Genet Evol *83*, 104353.
696 10.1016/j.meegid.2020.104353.
697 Camproux, A.C., Gautier, R., and Tuffery, P. (2004). A hidden markov model derived structural
698 alphabet for proteins. J Mol Biol *339*, 591-605. 10.1016/j.jmb.2004.04.005.
699 Finkel, Y., Mizrahi, O., Nachshon, A., Weingarten-Gabbay, S., Morgenstern, D., Yahalom-
700 Ronen, Y., Tamir, H., Achdout, H., Stein, D., Israeli, O., et al. (2021). The coding capacity of
701 SARS-CoV-2. Nature *589*, 125-130. 10.1038/s41586-020-2739-1.
702 Firth, A.E. (2020). A putative new SARS-CoV protein, 3c, encoded in an ORF overlapping
703 ORF3a. J Gen Virol *101*, 1085-1089. 10.1099/jgv.0.001469.
704 Firth, A.E., and Brierley, I. (2012). Non-canonical translation in RNA viruses. J Gen Virol *93*,
705 1385-1409. 10.1099/vir.0.042499-0.
706 Gleason, A.C., Ghadge, G., Chen, J., Sonobe, Y., and Roos, R.P. (2022). Machine learning
707 predicts translation initiation sites in neurologic diseases with nucleotide repeat expansions.
708 PLoS One *17*, e0256411. 10.1371/journal.pone.0256411.
709 Hachim, A., Gu, H., Kavian, O., Mori, M., Kwan, M.Y.W., Chan, W.H., Yau, Y.S., Chiu, S.S.,
710 Tsang, O.T.Y., Hui, D.S.C., et al. (2022). SARS-CoV-2 accessory proteins reveal distinct
711 serological signatures in children. Nat Commun *13*, 2951. 10.1038/s41467-022-30699-5.
712 Hayn, M., Hirschenberger, M., Koepke, L., Nchioua, R., Straub, J.H., Klute, S., Hunszinger,
713 V., Zech, F., Prelli Bozzo, C., Aftab, W., et al. (2021). Systematic functional analysis of SARS-
714 CoV-2 proteins uncovers viral innate immune antagonists and remaining vulnerabilities. Cell
715 Rep *35*, 109126. 10.1016/j.celrep.2021.109126.
716 Herrmann, A., Jungnickl, D., Cordsmeier, A., Peter, A.S., Uberla, K., and Ensser, A. (2021).
717 Cloning of a Passage-Free SARS-CoV-2 Genome and Mutagenesis Using Red Recombination.
718 Int J Mol Sci *22*. 10.3390/ijms221910188.
719 Jungreis, I., Nelson, C.W., Ardern, Z., Finkel, Y., Krogan, N.J., Sato, K., Ziebuhr, J., Stern-
720 Ginossar, N., Pavesi, A., Firth, A.E., et al. (2021a). Conflicting and ambiguous names of

721 overlapping ORFs in the SARS-CoV-2 genome: A homology-based resolution. Virology *558*,
722 145-151. 10.1016/j.virol.2021.02.013.
723 Jungreis, I., Sealfon, R., and Kellis, M. (2021b). SARS-CoV-2 gene content and COVID-19
724 mutation impact by comparing 44 Sarbecovirus genomes. Nat Commun *12*, 2642.
725 10.1038/s41467-021-22905-7.
726 Kimura, I., Konno, Y., Uriu, K., Hopfensperger, K., Sauter, D., Nakagawa, S., and Sato, K.
727 (2021). Sarbecovirus ORF6 proteins hamper induction of interferon signaling. Cell Rep *34*,
728 108916. 10.1016/j.celrep.2021.108916.
729 Kimura, I., Yamasoba, D., Nasser, H., Zahradnik, J., Kosugi, Y., Wu, J., Nagata, K., Uriu, K.,
730 Tanaka, Y.L., Ito, J., et al. (2022). The SARS-CoV-2 spike S375F mutation characterizes the
731 Omicron BA.1 variant. iScience *25*, 105720. 10.1016/j.isci.2022.105720.
732 Konno, Y., Kimura, I., Uriu, K., Fukushi, M., Irie, T., Koyanagi, Y., Sauter, D., Gifford, R.J.,
733 Consortium, U.-C., Nakagawa, S., and Sato, K. (2020). SARS-CoV-2 ORF3b Is a Potent
734 Interferon Antagonist Whose Activity Is Increased by a Naturally Occurring Elongation
735 Variant. Cell Rep *32*, 108185. 10.1016/j.celrep.2020.108185.
736 Kopecky-Bromberg, S.A., Martinez-Sobrido, L., Frieman, M., Baric, R.A., and Palese, P.
737 (2007). Severe acute respiratory syndrome coronavirus open reading frame (ORF) 3b, ORF 6,
738 and nucleocapsid proteins function as interferon antagonists. J Virol *81*, 548-557.
739 10.1128/JVI.01782-06.
740 Krogh, A., Larsson, B., von Heijne, G., and Sonnhammer, E.L. (2001). Predicting
741 transmembrane protein topology with a hidden Markov model: application to complete
742 genomes. J Mol Biol *305*, 567-580. 10.1006/jmbi.2000.4315.
743 Li, J.Y., Liao, C.H., Wang, Q., Tan, Y.J., Luo, R., Qiu, Y., and Ge, X.Y. (2020). The ORF6,
744 ORF8 and nucleocapsid proteins of SARS-CoV-2 inhibit type I interferon signaling pathway.
745 Virus Res *286*, 198074. 10.1016/j.virusres.2020.198074.
746 Li, X., Hou, P., Ma, W., Wang, X., Wang, H., Yu, Z., Chang, H., Wang, T., Jin, S., Wang, X.,
747 et al. (2022). SARS-CoV-2 ORF10 suppresses the antiviral innate immune response by
748 degrading MAVS through mitophagy. Cell Mol Immunol *19*, 67-78. 10.1038/s41423-021-
749 00807-4.
750 Matsuyama, S., Nao, N., Shirato, K., Kawase, M., Saito, S., Takayama, I., Nagata, N., Sekizuka,
751 T., Katoh, H., Kato, F., et al. (2020). Enhanced isolation of SARS-CoV-2 by TMPRSS2-
752 expressing cells. Proc Natl Acad Sci U S A *117*, 7001-7003. 10.1073/pnas.2002589117.
753 Min, Y.Q., Huang, M., Sun, X., Deng, F., Wang, H., and Ning, Y.J. (2021). Immune evasion
754 of SARS-CoV-2 from interferon antiviral system. Comput Struct Biotechnol J *19*, 4217-4225.
755 10.1016/j.csbj.2021.07.023.
756 Miorin, L., Kehrer, T., Sanchez-Aparicio, M.T., Zhang, K., Cohen, P., Patel, R.S., Cupic, A.,
757 Makio, T., Mei, M., Moreno, E., et al. (2020). SARS-CoV-2 Orf6 hijacks Nup98 to block STAT
758 nuclear import and antagonize interferon signaling. Proc Natl Acad Sci U S A *117*, 28344-
759 28354. 10.1073/pnas.2016650117.
760 Nelson, C.W., Ardern, Z., Goldberg, T.L., Meng, C., Kuo, C.H., Ludwig, C., Kolokotronis,
761 S.O., and Wei, X. (2020). Dynamically evolving novel overlapping gene as a factor in the
762 SARS-CoV-2 pandemic. Elife *9*. 10.7554/eLife.59633.
763 Oulas, A., Zanti, M., Tomazou, M., Zachariou, M., Minadakis, G., Bourdakou, M.M., Pavlidis,
764 P., and Spyrou, G.M. (2021). Generalized linear models provide a measure of virulence for
765 specific mutations in SARS-CoV-2 strains. PLoS One *16*, e0238665.
766 10.1371/journal.pone.0238665.
767 Pavesi, A. (2020). New insights into the evolutionary features of viral overlapping genes by
768 discriminant analysis. Virology *546*, 51-66. 10.1016/j.virol.2020.03.007.
769 Strahle, L., Garcin, D., and Kolakofsky, D. (2006). Sendai virus defective-interfering genomes
770 and the activation of interferon-beta. Virology *351*, 101-111. 10.1016/j.virol.2006.03.022.

771 Tischer, B.K., von Einem, J., Kaufer, B., and Osterrieder, N. (2006). Two-step red-mediated
772 recombination for versatile high-efficiency markerless DNA manipulation in Escherichia coli.
773 Biotechniques *40*, 191-197. 10.2144/000112096.
774 Torii, S., Ono, C., Suzuki, R., Morioka, Y., Anzai, I., Fauzyah, Y., Maeda, Y., Kamitani, W.,
775 Fukuhara, T., and Matsuura, Y. (2021). Establishment of a reverse genetics system for SARS-
776 CoV-2 using circular polymerase extension reaction. Cell Rep *35*, 109014.
777 10.1016/j.celrep.2021.109014.
778 Varga, Z.T., Grant, A., Manicassamy, B., and Palese, P. (2012). Influenza virus protein PB1-
779 F2 inhibits the induction of type I interferon by binding to MAVS and decreasing mitochondrial
780 membrane potential. J Virol *86*, 8359-8366. 10.1128/JVI.01122-12.
781 Varga, Z.T., Ramos, I., Hai, R., Schmolke, M., Garcia-Sastre, A., Fernandez-Sesma, A., and
782 Palese, P. (2011). The influenza virus protein PB1-F2 inhibits the induction of type I interferon
783 at the level of the MAVS adaptor protein. PLoS Pathog *7*, e1002067.
784 10.1371/journal.ppat.1002067.
785 Xia, H., Cao, Z., Xie, X., Zhang, X., Chen, J.Y., Wang, H., Menachery, V.D., Rajsbaum, R.,
786 and Shi, P.Y. (2020). Evasion of Type I Interferon by SARS-CoV-2. Cell Rep *33*, 108234.
787 10.1016/j.celrep.2020.108234.

788

Fig. 1

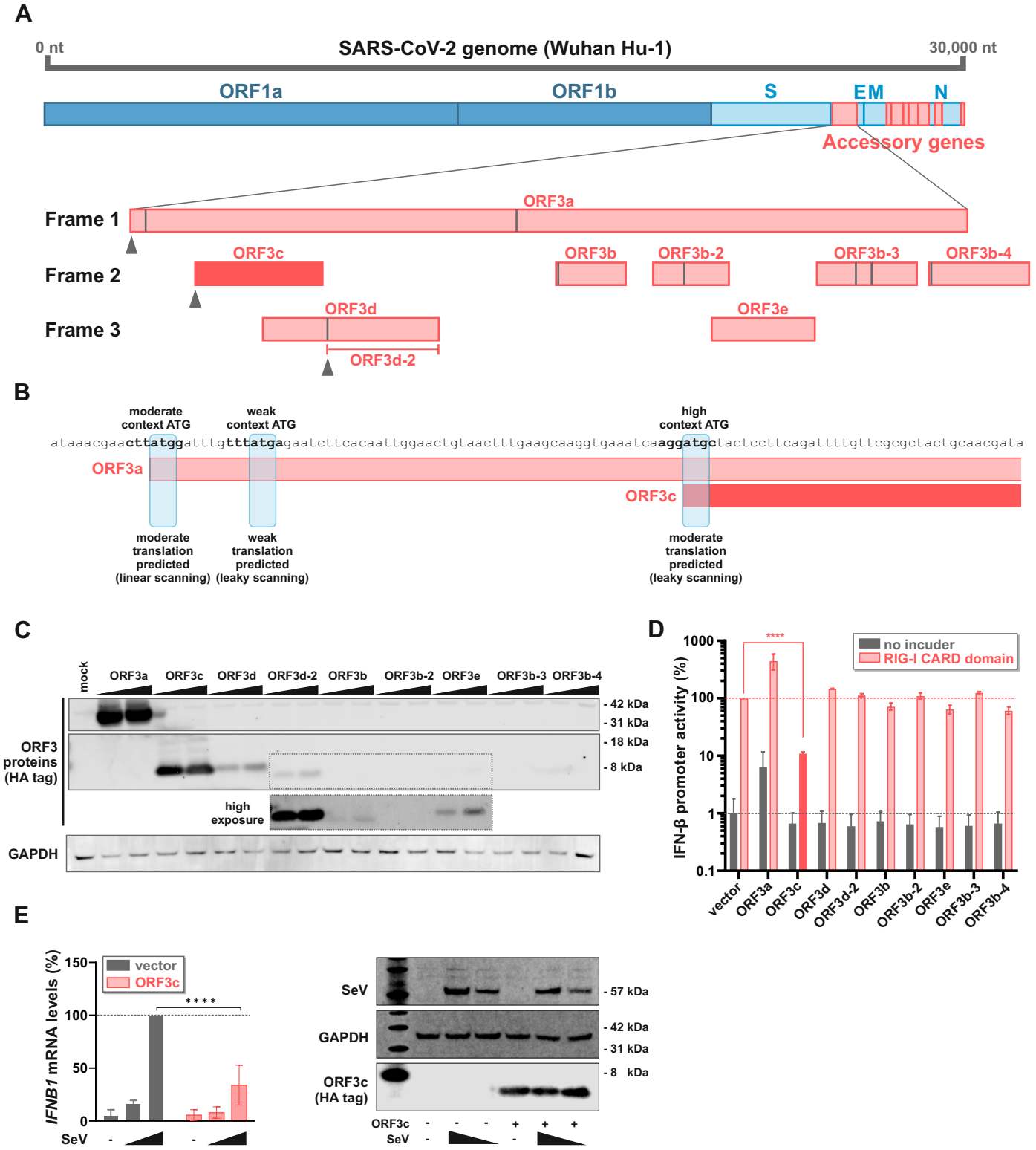
A
0 nt
SARS-CoV-2 genome (Wuhan Hu-1)
30,000 nt
ORF1a
ORF1b
S
EM
N
Accessory genes
Frame 1
ORF3a
Frame 2
ORF3c
ORF3b
ORF3b-2
ORF3b-3
ORF3b-4
Frame 3
ORF3d
ORF3e
ORF3d-2
B
moderate context ATG
weak context ATG
high context ATG
ataaacgaacttatggatttgtttatgagaatcttcacaattggaactgtaactttgaagcaaggtgaaatcaaggatgctactccttcagattttgttcgcgctactgcaacgata
ORF3a
ORF3c
moderate translation predicted (linear scanning)
weak translation predicted (leaky scanning)
moderate translation predicted (leaky scanning)
C
mock
ORF3a
ORF3c
ORF3d
ORF3d-2
ORF3b
ORF3b-2
ORF3e
ORF3b-3
ORF3b-4
ORF3 proteins (HA tag)
high exposure
GAPDH
- 42 kDa
- 31 kDa
- 18 kDa
- 8 kDa
D
no incuder
RIG-I CARD domain
IFN-β promoter activity (%)
1000
100
10
1
0.1
****
vector
ORF3a
ORF3c
ORF3d
ORF3d-2
ORF3b
ORF3b-2
ORF3e
ORF3b-3
ORF3b-4
E
vector
ORF3c
IFNB1 mRNA levels (%)
150
100
50
0
****
SeV
SeV
GAPDH
ORF3c (HA tag)
- 57 kDa
- 42 kDa
- 31 kDa
- 8 kDa
ORF3c
SeV

Fig. 2

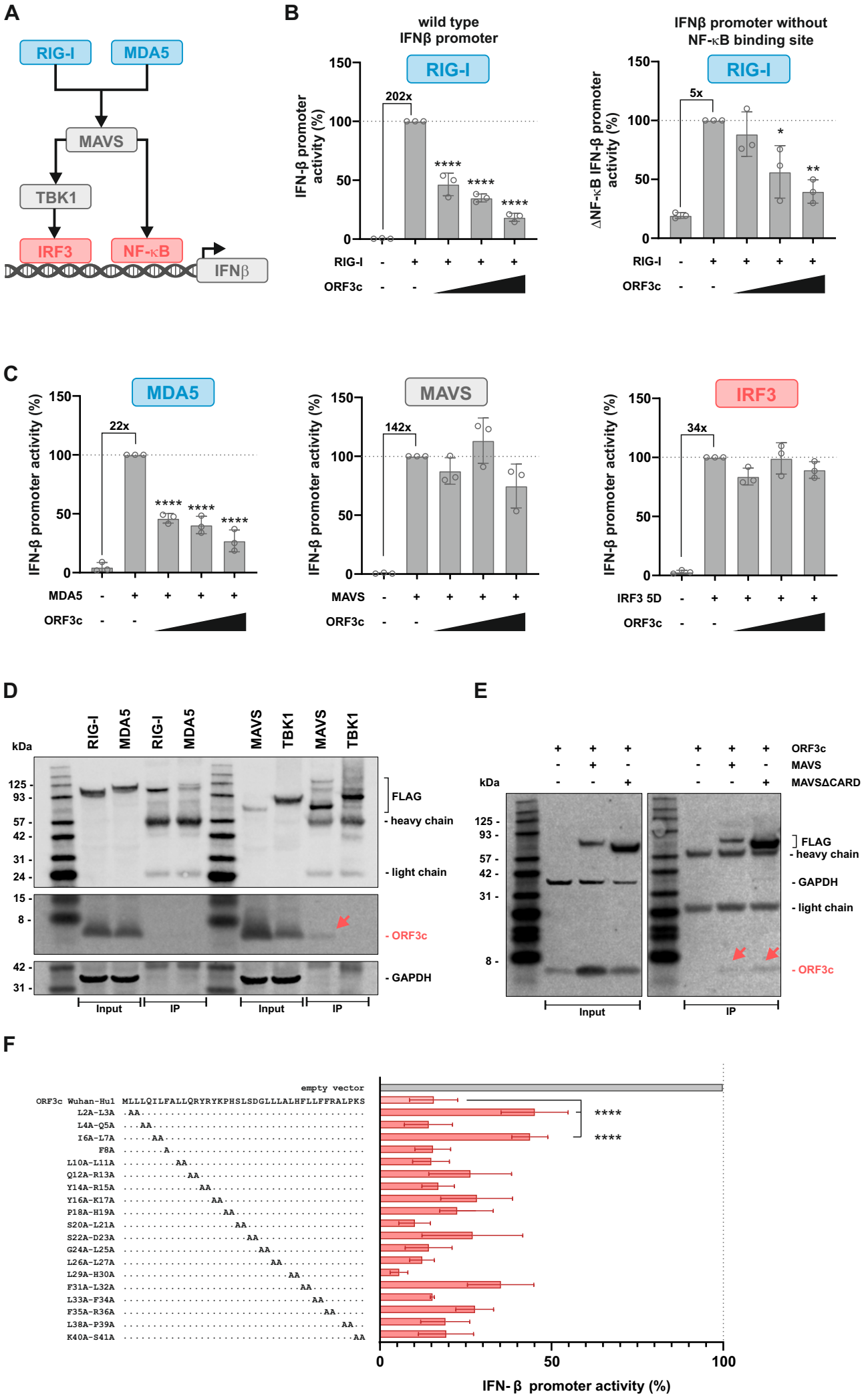
A
RIG-I
MDA5
MAVS
TBK1
IRF3
NF-κB
IFNβ
B
wild type IFNβ promoter
RIG-I
IFN-β promoter activity (%)
202x
RIG-I
ORF3c
IFNβ promoter without NF-κB binding site
ΔNF-κB IFN-β promoter activity (%)
5x
C
MDA5
22x
MAVS
142x
IRF3
34x
IFN-β promoter activity (%)
MDA5
MAVS
IRF3 5D
ORF3c
D
kDa
RIG-I
MDA5
MAVS
TBK1
FLAG
- heavy chain
- light chain
- ORF3c
- GAPDH
Input
IP
E
ORF3c
MAVS
MAVSΔCARD
- GAPDH
F
empty vector
ORF3c Wuhan-Hu1 MLLLQILFALLQRYRYKPHSLSDGLLLALHFLLFFRALPKS
L2A-L3A
L4A-Q5A
I6A-L7A
F8A
L10A-L11A
Q12A-R13A
Y14A-R15A
Y16A-K17A
P18A-H19A
S20A-L21A
S22A-D23A
G24A-L25A
L26A-L27A
L29A-H30A
F31A-L32A
L33A-F34A
F35A-R36A
L38A-P39A
K40A-S41A
IFN-β promoter activity (%)

Fig. 3

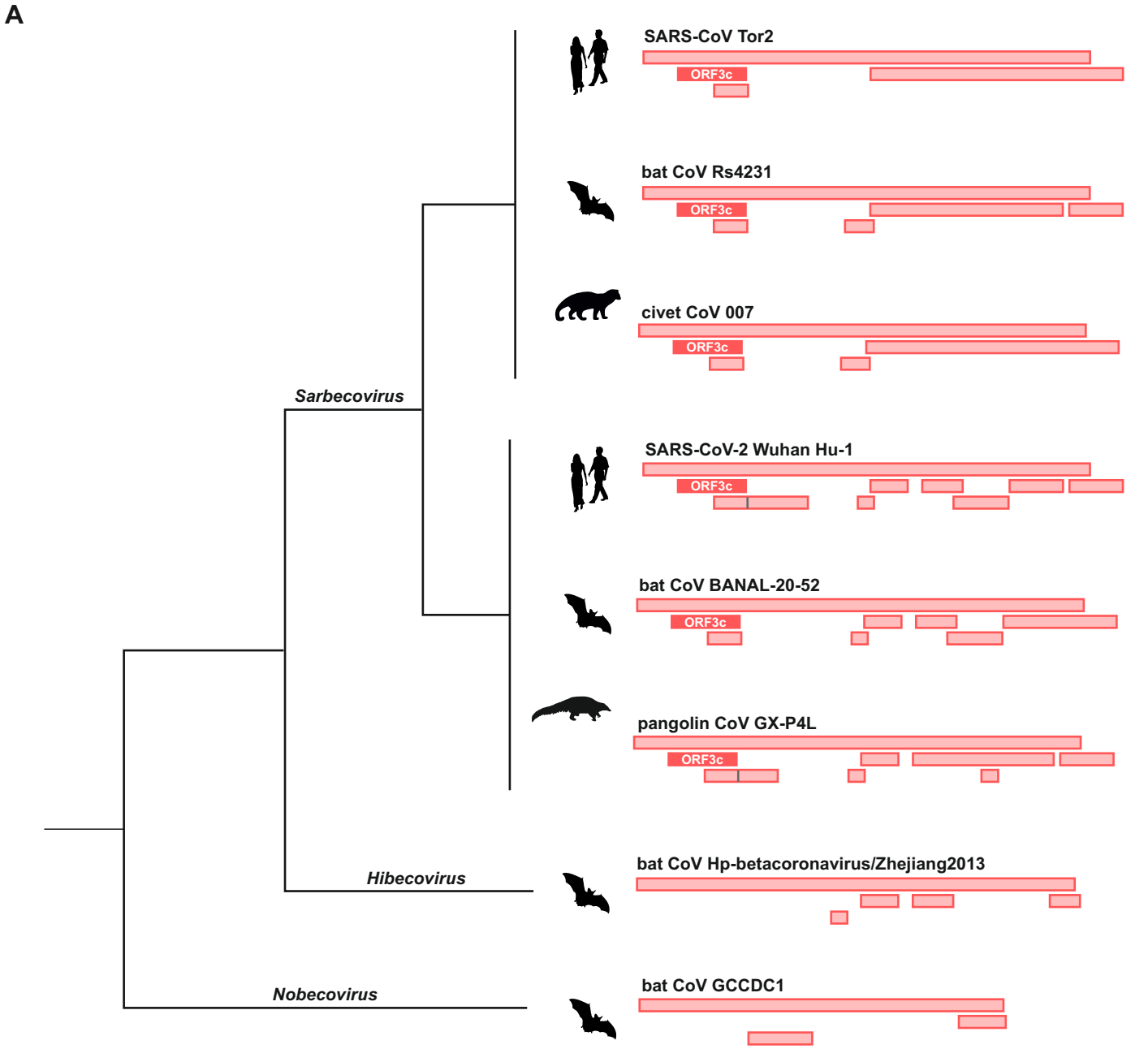

B

```
                1                                          41
Wuhan Hu-1      MLLLQILFAL LQRYRYKPHS LSDGLLLALH FLLFFRALPK S

RmYN02          .......... .......... .......... .......... .
BANAL-20-103    .......... .......... .......... .....K.... .
BANAL-20-236    .......... .......... .......... .....K.... .
RaTG13          .......... .......... .......... .....K...R .
RShSTT200       ....H..... .......... .......... .......... .
RShSTT182       ....H..... .......... .......... .......... .
BANAL-20-52     .......... P......... .......... .......... .
ZXC21           .......... ..Q....... .........Q .....K..Q. -

P2S             .......... .......... .......... .....K.... -
P1E             .......... .......... .......... .......... -
P4L             .......... .......... .......... .....T.... -

Tor2            .....V..M. Q......... .......... .......... -
SZ3             .....V..M. Q......... .......... .......... -

Rs4231          .....V..M. Q.....R... .......... .......... -

007             ...M.V..V. Q......... .......... .......... -
```

SARS-CoV-2 cluster

SARS-CoV cluster

C

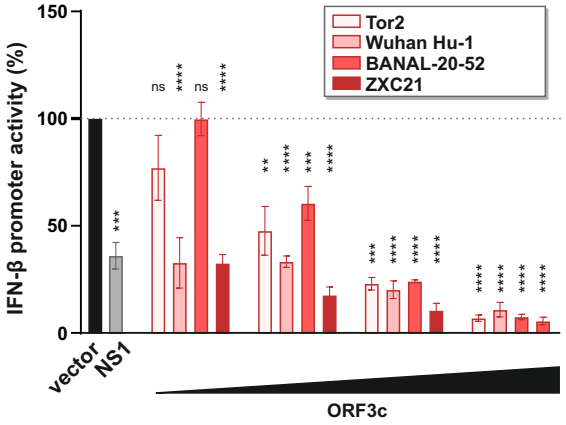

Fig. 4

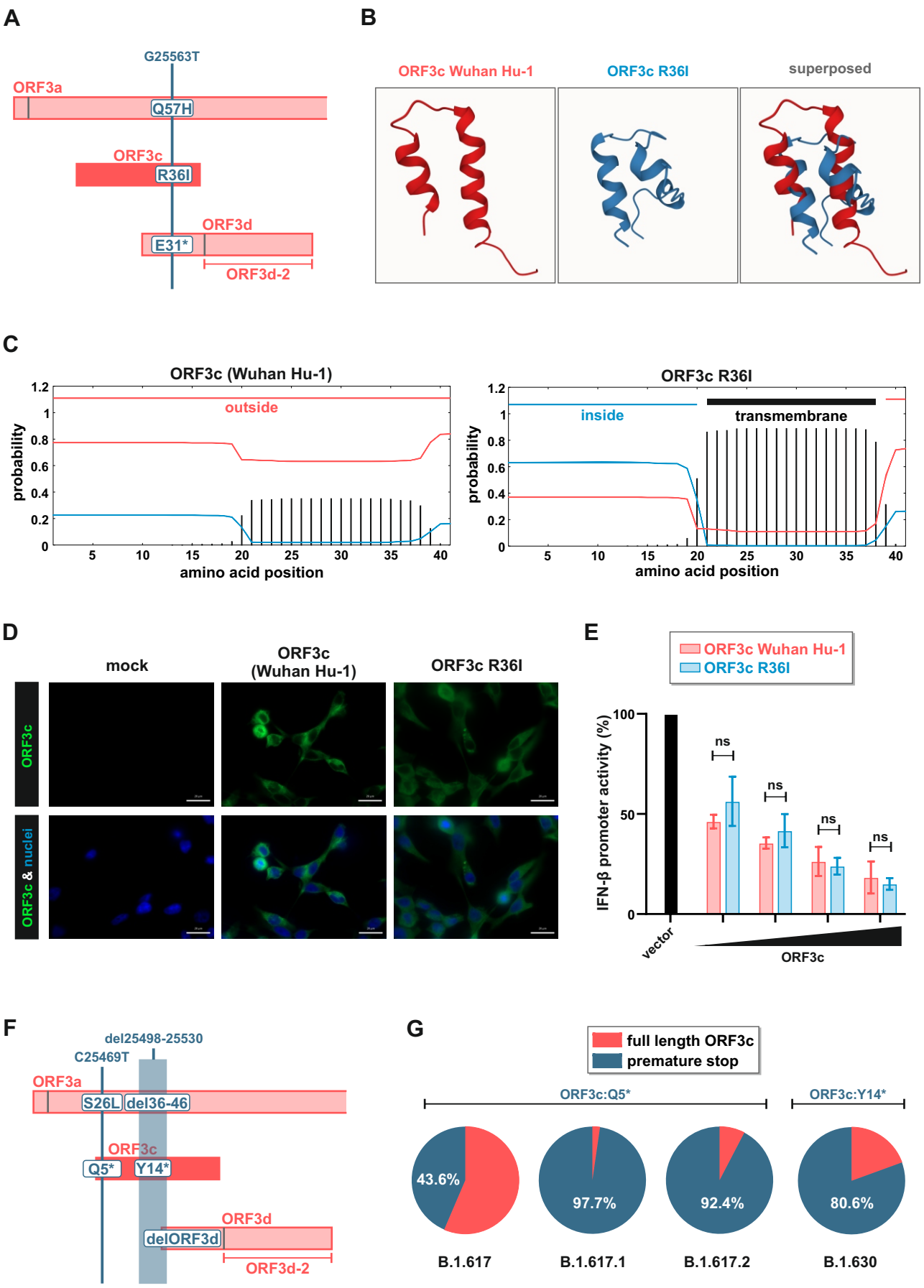
A
G25563T
ORF3a
Q57H
ORF3c
R36I
ORF3d
E31*
ORF3d-2
B
ORF3c Wuhan Hu-1
ORF3c R36I
superposed
C
ORF3c (Wuhan Hu-1)
outside
probability
amino acid position
ORF3c R36I
inside
transmembrane
probability
amino acid position
D
mock
ORF3c (Wuhan Hu-1)
ORF3c R36I
ORF3c
ORF3c & nuclei
E
ORF3c Wuhan Hu-1
ORF3c R36I
IFN-β promoter activity (%)
ns
vector
ORF3c
F
del25498-25530
C25469T
ORF3a
S26L
del36-46
ORF3c
Q5*
Y14*
ORF3d
delORF3d
ORF3d-2
G
full length ORF3c
premature stop
ORF3c:Q5*
ORF3c:Y14*
43.6%
97.7%
92.4%
80.6%
B.1.617
B.1.617.1
B.1.617.2
B.1.630

Fig. 5

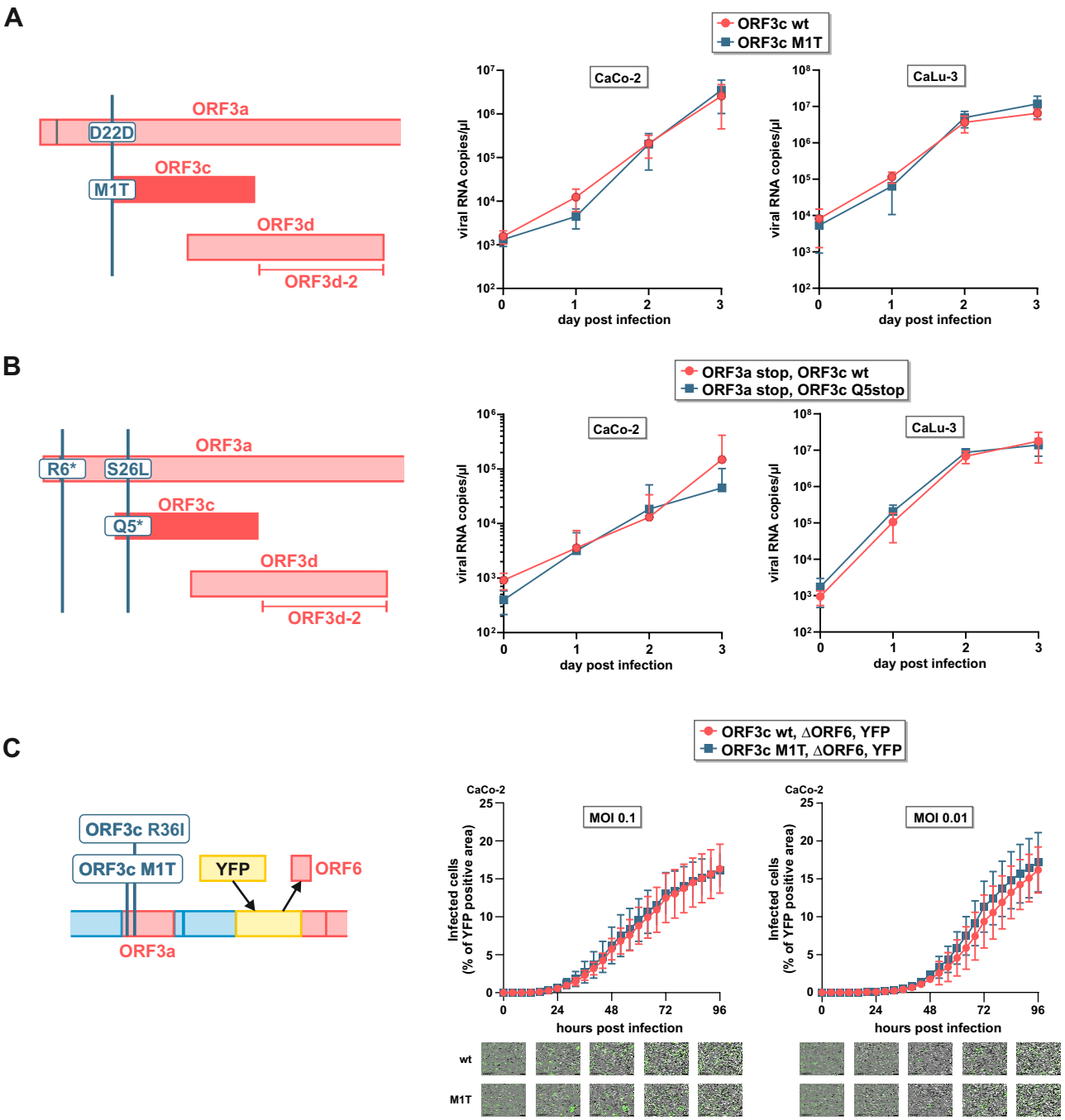
A
ORF3a
D22D
ORF3c
M1T
ORF3d
ORF3d-2
ORF3c wt
ORF3c M1T
CaCo-2
CaLu-3
viral RNA copies/µl
day post infection
B
ORF3a
R6*
S26L
ORF3c
Q5*
ORF3d
ORF3d-2
ORF3a stop, ORF3c wt
ORF3a stop, ORF3c Q5stop
CaCo-2
CaLu-3
viral RNA copies/µl
day post infection
C
ORF3c R36I
ORF3c M1T
YFP
ORF6
ORF3a
ORF3c wt, ΔORF6, YFP
ORF3c M1T, ΔORF6, YFP
CaCo-2
MOI 0.1
MOI 0.01
Infected cells
(% of YFP positive area)
hours post infection
wt
M1T

Fig. S1

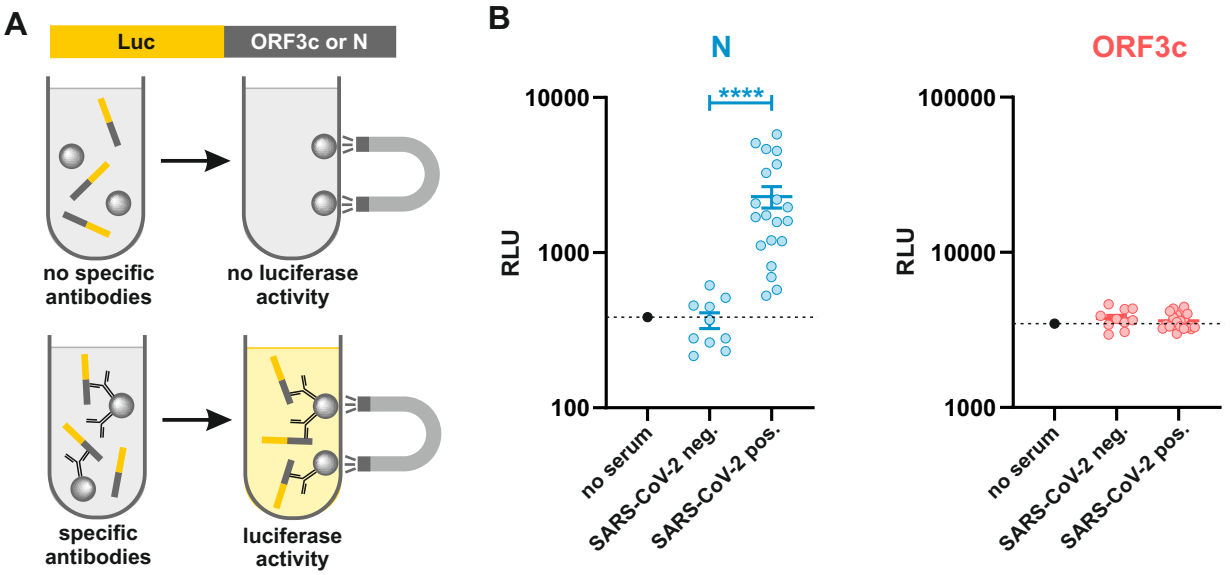
A
Luc
ORF3c or N
no specific antibodies
no luciferase activity
specific antibodies
luciferase activity
B
N
ORF3c
RLU
10000
1000
100
****
100000
10000
1000
no serum
SARS-CoV-2 neg.
SARS-CoV-2 pos.